VIP NMR Spectroscopy Very Important Paper

DOI: 10.1002/anie.201305184

Molecular Mechanism of Prion Protein Oligomerization at Atomic Resolution**

*Kai Schlepckow and Harald Schwalbe**

Dedicated to Professor Werner Müller-Esterl on the occasion of his 65th birthday

Misfolding of the cellular isoform of the prion protein (PrP^C) to the abnormal aggregated isoform (PrP^{Sc}) is the central hallmark of transmissible spongiform encephalopathies (TSEs) also known as prion diseases.[1,2] During misfolding, major structural rearrangement occurs encompassing the entire polypeptide chain. The monomeric mainly α-helical PrP^C converts into polymeric PrP^{Sc} largely enriched in β-sheet structure.[3,4] The three-dimensional (3D) structures of PrP^C from different species have revealed fold conservation with only little interspecies structural variation.[5,6] Similarly, also the unfolded states of the human and murine prion proteins show only subtle differences.[7,8] Detailed structural studies of PrP^{Sc} have been much more difficult. Recently, mass spectrometry in conjunction with hydrogen/deuterium exchange,[9,10] EPR,[11] liquid-state[12] and solid-state NMR studies[13] have provided consistent structural insight into PrP^{Sc}-like assemblies. However, site-resolved information regarding the pathway PrP monomers follow to give rise to these macromolecular assemblies is still lacking. Such information is very precious since it is established that for prion diseases as well as several other neurodegenerative diseases[14] the associated proteins exert their detrimental cytotoxic effects by self-assembly into distinct oligomeric states. Therefore, it is imperative to characterize their formation pathways to devise successful small-molecule-based approaches preventing oligomerization.

Here, we overcome the limited structural resolution in previous mechanistic studies[15–18] by applying time-resolved NMR spectroscopy and characterize the oligomerization kinetics of recombinant murine PrP (mPrP) at single-residue level. Oligomerization is initiated from 4 M urea pH 2.0, conditions commonly employed in investigations of PrP oligomerization.[15–19] It involves two distinct steps: in the first step, oligomers of order 5–8 are formed as evidenced by sodium dodecyl sulfate polyacrylamide gel electrophoresis (SDS-PAGE). The size of the oligomers is independent of 1) protein concentration differences spanning one order of magnitude, 2) presence of reducing agent, and 3) temperature denaturation (see Figure S1 in the Supporting Information). Having established that oligomers of finite size distribution form under these conditions, a detailed NMR characterization was conducted, since the two-dimensional (2D) ^1H, ^{15}N-correlation spectrum (HSQC) exhibits a large number of resolved signals (Figure S2) and the process is sufficiently slow to acquire 2D spectra. Comparison of resonance intensities at 4 M urea and of the completely unfolded state at 8 M urea shows that almost the entire polypeptide sequence exhibits significantly reduced signal intensities under the oligomerization conditions (Figure 1 A).

The mPrP oligomerization kinetics was measured over a period of five days. No significant changes in resonance line widths were observed (Figure S3) indicating that exchange between mPrP monomers and oligomers occurs on slower timescales and that the disappearance of peaks in HSQC spectra corresponds to depletion of monomeric mPrP. We do not observe a lag phase indicative of classical nucleation-dependent polymerization[20] in agreement with previous studies.[15,19] In the first kinetic spectrum residues in close proximity to the disulfide-forming cysteines C179 and C214, for example, V176 and Q212, are broadened beyond detection. This and the observation that decreases in peak intensity compared to the fully unfolded state are most pronounced for the sequence stretch enclosed by the disulfide bond (Figure 1 A) suggest that molten globule-type conformational dynamics[21,22] for this part of the polypeptide chain play a significant role in establishing intermolecular contacts during oligomerization.[23]

We followed the kinetics of the loss of mPrP monomers for a total of 75 individual amino acids (Figure 1 B–F). As expected for an oligomerization reaction which is not unfolding-limited the data cannot be described by first-order kinetics.[24] We analyzed the kinetic traces of 67 residues for which reliable fits could be obtained with the following function describing the time-dependent loss of monomers $m^i(t)$ monitored on residue i upon self-assembly in the case of an irreversible two-state transition of nth order [Eq. (1)],

$$m^i(t) = m^i(0)\left(\frac{1}{1+t/\tau}\right)^{1/(n-1)} \quad (1)$$

[*] Dr. K. Schlepckow, Prof. Dr. H. Schwalbe
Institut für Organische Chemie und Chemische Biologie
Zentrum für Biomolekulare Magnetische Resonanz (BMRZ)
Johann Wolfgang Goethe-Universität Frankfurt am Main
Max-von-Laue-Strasse 7, 60438 Frankfurt am Main (Germany)
E-mail: schwalbe@nmr.uni-frankfurt.de
Homepage: http://schwalbe.org.chemie.uni-frankfurt.de

[**] Financial support of this work through the German Research Foundation (DFG, grant number Schw701/9-1,9-2) and through the state of Hessen (BMRZ) is gratefully acknowledged. H.S. is a member of the DFG-funded Cluster of Excellence: Macromolecular Complexes. We thank Nils Walter for helpful discussions, Julia Wirmer-Bartoschek for critically reading the manuscript, and Sven Warhaut for preparation of an NMR sample.

Supporting information for this article is available on the WWW under http://dx.doi.org/10.1002/anie.201305184.

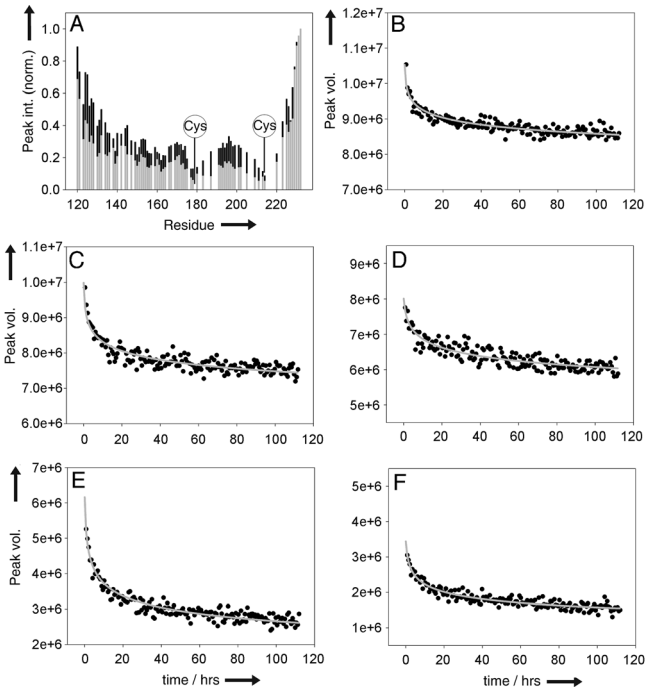

Figure 1. Oligomerization of murine PrP at a concentration of 700 μM. A) Normalized peak intensities at 8 M urea (black bars) and 4 M urea (gray bars), pH 2.0. Positions of disulfide-forming cysteines are indicated. Data at 8 M urea were acquired from a separate sample. In both data sets, the peak intensity of the C-terminal residue S232 was set to unity. B–F) Real-time NMR kinetic traces showing the oligomerization-induced decrease in the monomeric population for G126 (B), N153 (C), Q172 (D), G195 (E), and M213 (F). Gray lines indicate nonlinear least-squares fits of the data according to Equation (1).

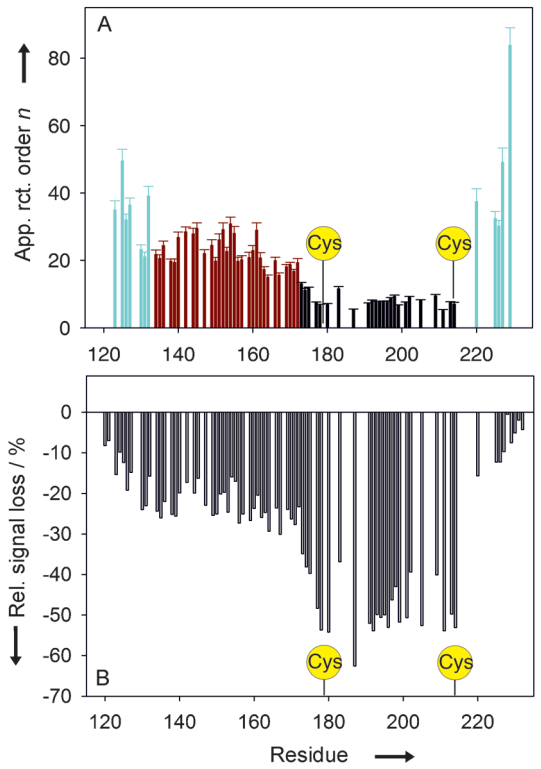

Figure 2. Oligomerization of mPrP at a concentration of 700 μM. A) Sequence-dependent apparent reaction order *n* as determined from fitting of the kinetic data as shown in Figure 1 B–F to Equation (1). Color coding refers to the determination of the size distribution of oligomeric species (cf. Table 1). Residue groups 1, 2, and 3 are denoted by black, dark red, and cyan colors, respectively. B) Sequence-dependent relative loss in peak volume over a period of five days upon mPrP oligomerization. Positions of disulfide-forming cysteines are indicated.

where $m^i(0)$, τ, and n correspond to the concentration of monomer monitored on residue i at time zero, the apparent time constant of the process, and the apparent reaction order, respectively.[25] The probability of n molecules colliding at the same time to yield an oligomer composed of n monomers with $n > 2$ is very low and therefore oligomerization proceeds as a sequence of bimolecular reactions. In the case of an irreversible transition with only weakly populated intermediates the apparent reaction order n as extracted from a fit of monomer-loss data to Equation (1) would consequently yield $n \approx 2$. In contrast, we find apparent reaction orders of $n > 5$ with substantial variation of reaction orders of oligomerization for different residues (Figure 2 A).

The lowest reaction orders are found for residues residing in the loop enclosed by cysteines C179 and C214 with $5 < n < 12$. Higher reactions orders with $n > 12$ are identified toward the chain termini with the very N- and C-terminal residues even showing reaction orders of $n > 40$. These observations cannot be explained by a two-state transition but invoke the significant population of intermediates during oligomerization[17,25,26] and allow us to differentiate between molecular interactions important for oligomerization from those molecular interactions that feature in further self-assembly of the initially formed oligomers.

The residue-specific changes reflect changes in the timescales of rigidification of different parts of the polypeptide chain upon oligomerization and subsequent self-assembly. Major involvement of the disulfide loop residues during oligomerization suggests that they experience significant rigidification in the initial oligomerization step whereas the remainder of the chain remains largely flexible. The remainder of the chain becomes more rigid upon the second step of self-assembly of preformed oligomers. This behavior also explains the observation that the relative signal loss detected in the oligomerization kinetics is dramatically nonuniform across the polypeptide sequence with the disulfide loop region exhibiting the most pronounced signal decrease (Figure 2 B). Recasting [Eq. (1)] allows us to extract the apparent time constant of the overall oligomerization process yielding $\tau = 0.45 \pm 0.05$ h (Figure S4).

Time-dependent UV absorption difference spectroscopy shows that self-assembly of preformed oligomers is accompanied by major burial of tyrosine side-chains during self-assembly (Figure S5).[27] All 10 tyrosine residues in the polypeptide sequence are found outside the disulfide loop. The monitored shielding of tyrosine residues from solvent is well-supported by the observation that signal intensities for peaks stemming from the N- and C-terminal regions preceding and succeeding the disulfide loop, respectively, are dramatically reduced after one year (Figure S6). Therefore,

polypeptide chain rigidification outside the disulfide loop is not complete at the end of the kinetic measurements but proceeds on a substantially slower timescale after initial oligomerization. Congo red dye binding experiments show that the nature of formed PrP assemblies is amyloid-like (Figure S7).[28]

It should be stressed that only the intensity but not the linewidth changes over the course of the NMR experiment. From NMR spectroscopy alone, we cannot strictly rule out substantial differential dynamics for different groups of residues leading to differential broadening of lines beyond detection. However, as shown previously, flexible parts remain NMR-visible in structures with oligomeric cores.[29] Therefore, we interpret the differences in reaction order from different parts of the polypeptide chain (Figure 2A) by defining distinct groups of oligomers in order to quantify their sizes and effective concentrations (Table 1).

Table 1: Determination of the average sizes and effective concentrations of ensembles of oligomeric species. Residues were grouped according to their apparent reaction orders (cf. Figure 2A and the Experimental Section in the Supporting Information). The first stage of oligomerization refers to initial oligomerization whereas the second stage indicates self-assembly of preformed oligomers. Given errors are standard deviations.

	Group 1	Group 2	Group 3
Oligomerization stage	1st	2nd	2nd
Average reaction order (no. of monomers)	8.3 ± 1.9	22.4 ± 4.5	39.1 ± 16.5
Average MW [kDa]	110 ± 25	300 ± 60	520 ± 220
Average signal loss [%]	−48.3 ± 6.9	−23.4 ± 3.7	−15.2 ± 4.9
Fraction of initial monomer concentration [%]	24.9	8.2	15.2
Effective concentration [μM]	21	2.6	2.7

Based on our analysis, oligomeric species of up to 40-mers can be identified and their effective concentrations can be estimated. Residues of group 1 mainly include the disulfide loop region and loose about 48% of the peak volume within the course of the measurement, that is, 48% of the monomers oligomerize into octamers and higher-order oligomeric assemblies while 52% remain in the monomeric state. Residues belonging to group 2 encompass sequence region 134–172 and loose on average about 23% of their signal. Consequently, about 25% of the signal loss detected for group 1 residues results from the formation of octamers. Based on an initial monomer concentration of 700 μM an estimate of the effective concentration of octamers yields 21 μM. Average sizes and effective concentrations of higher-order oligomeric species resulting from self-assembly of initially formed oligomers were calculated accordingly. The effective concentration of group 3 oligomers might be lower than given in Table 1 as we cannot exclude the formation of even larger species which escape detection in our experiments.

Based on these findings, we propose a model for prion protein oligomerization and self-assembly. In this model, initial oligomerization proceeds from a largely unfolded state. Interconversion rates in the conformational ensemble are close to the exchange timescale of molten globule states and initial intermolecular contacts are mediated by the sequence stretch enclosed by disulfide-forming cysteines C179 and C214 (Figure 3, 1st stage) matching previous studies on PrP oligomerization and fibrillation (Figure S8).[9–13,30]

The strikingly nonuniform changes in the entire polypeptide chain monitored at residue resolution (Figure 2A,B) reveal that the sequence regions outside the disulfide loop do not remain flexible throughout oligomerization but undergo substantial rigidification during slow self-assembly of preformed oligomers (Figure 3, 2nd stage). This second oligomerization step is accompanied by significant burial of tyrosine side-chains which stresses the relevance of hydrophobic interactions in mediating higher-order oligomerization events. The nonuniform behavior of the polypeptide sequence during oligomerization underlines that substantial refolding of native monomeric PrP is required for conversion into β-

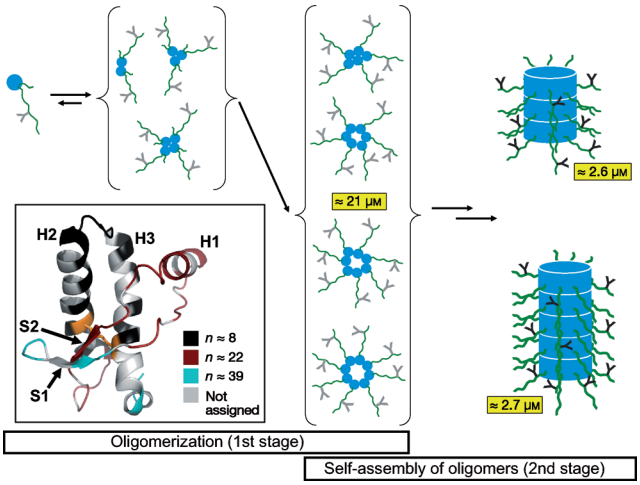

Figure 3. Model for oligomerization and subsequent self-assembly of oligomers. The disulfide loop region and the N- and C-terminal sequence stretches are indicated by blue circles/disks and green lines, respectively. Tyrosine residues are depicted by their one-letter code (Y). Initial oligomerization is mediated by the disulfide loop residues (1st stage). Oligomeric species up to tetramers are not resistant to denaturing conditions as employed during SDS-PAGE analysis (Figure S1). Self-assembly to congo-red-active, that is, amyloid-like structures may involve multiple steps and leads to a polydisperse distribution of structures (2nd stage, only two structures shown: trimer of octamers and pentamer of octamers corresponding to group 2 and group 3 ensembles of oligomeric species in Table 1, respectively). Effective concentrations (yellow boxes) were taken from Table 1. Tyrosine residues only become shielded from solvent upon slow self-assembly of preformed oligomers (indicated by light gray (not shielded) and dark gray (shielded) colors). The increasing extent of polypeptide chain rigidification upon self-assembly of oligomers is schematically shown by increasingly thicker N-terminal tails for increasingly larger structures. For simplicity, C-terminal tails are only shown for species up to tetramers and tyrosine residues are only indicated for a subset of the tails in the self-assembled oligomers. Association of oligomers as disk-like structures has been previously suggested.[31] The inset shows apparent reaction orders plotted onto the 3D structure of native mPrP[5] with the same color coding as given in Figure 2A except that unassigned residues and the disulfide bridge are colored gray and orange, respectively. Locations of β-strands (S1–S2) and α-helices (H1–H3) are indicated.

sheet-enriched oligomeric structures such as PrP^{Sc} (Figure 3, inset).

We conclude that our experiments yield unique insight into the distribution of initially formed oligomers and how they interact to form higher-order assemblies (Table 1). The analysis reveals significant oligomer polydispersity which is in general accordance with simulations of monomer-loss kinetics under conditions where oligomerization is not unfolding-limited.[24] Crucially, our data allows us to determine the effective concentrations of distinct ensembles of oligomeric species. We thus gain access to important parameters such as size, concentration, and stabilizing intermolecular interactions of oligomeric species which may constitute key intermediates during PrP pathogenesis. We are now in the position to investigate the effect of disease-associated single-point mutations on the kinetics of oligomer formation which will be subject of further studies. The outlined approach of analyzing the sequence-dependent monomer-loss kinetics should be broadly applicable to a wide range of proteins implicated in neurodegenerative diseases and provide long-sought mechanistic insight into how these proteins self-assemble into oligomeric and fibrillar structures. We anticipate that the insights gained in the current study will help elucidate the molecular details of protein aggregation underlying protein misfolding diseases.

Received: June 17, 2013
Published online: August 9, 2013

Keywords: kinetics · mechanistic studies · NMR spectroscopy · oligomerization · prion proteins

[1] S. B. Prusiner, *Science* **1982**, *216*, 136.
[2] S. B. Prusiner, *Proc. Natl. Acad. Sci. USA* **1998**, *95*, 13363.
[3] B. W. Caughey, A. Dong, K. S. Bhat, D. Ernst, S. F. Hayes, W. S. Caughey, *Biochemistry* **1991**, *30*, 7672.
[4] K. M. Pan, M. Baldwin, J. Nguyen, M. Gasset, A. Serban, D. Groth, I. Mehlhorn, Z. Huang, R. J. Fletterick, F. E. Cohen, et al., *Proc. Natl. Acad. Sci. USA* **1993**, *90*, 10962.
[5] R. Riek, S. Hornemann, G. Wider, M. Billeter, R. Glockshuber, K. Wüthrich, *Nature* **1996**, *382*, 180.
[6] D. A. Lysek, C. Schorn, L. G. Nivon, V. Esteve-Moya, B. Christen, L. Calzolai, C. von Schroetter, F. Fiorito, T. Herrmann, P. Güntert, K. Wüthrich, *Proc. Natl. Acad. Sci. USA* **2005**, *102*, 640.
[7] C. Gerum, R. Silvers, J. Wirmer-Bartoschek, H. Schwalbe, *Angew. Chem.* **2009**, *121*, 9616; *Angew. Chem. Int. Ed.* **2009**, *48*, 9452.
[8] C. Gerum, K. Schlepckow, H. Schwalbe, *J. Mol. Biol.* **2010**, *401*, 7.
[9] X. Lu, P. L. Wintrode, W. K. Surewicz, *Proc. Natl. Acad. Sci. USA* **2007**, *104*, 1510.
[10] V. Smirnovas, G. S. Baron, D. K. Offerdahl, G. J. Raymond, B. Caughey, W. K. Surewicz, *Nat. Struct. Mol. Biol.* **2011**, *18*, 504.
[11] N. J. Cobb, F. D. Sonnichsen, H. McHaourab, W. K. Surewicz, *Proc. Natl. Acad. Sci. USA* **2007**, *104*, 18946.
[12] J. Kumar, S. Sreeramulu, T. L. Schmidt, C. Richter, J. Vonck, A. Heckel, C. Glaubitz, H. Schwalbe, *ChemBioChem* **2010**, *11*, 1208.
[13] R. Tycko, R. Savtchenko, V. G. Ostapchenko, N. Makarava, I. V. Baskakov, *Biochemistry* **2010**, *49*, 9488.
[14] C. Haass, D. J. Selkoe, *Nat. Rev. Mol. Cell Biol.* **2007**, *8*, 101.
[15] W. Swietnicki, M. Morillas, S. G. Chen, P. Gambetti, W. K. Surewicz, *Biochemistry* **2000**, *39*, 424.
[16] I. V. Baskakov, G. Legname, M. A. Baldwin, S. B. Prusiner, F. E. Cohen, *J. Biol. Chem.* **2002**, *277*, 21140.
[17] F. Sokolowski, A. J. Modler, R. Masuch, D. Zirwer, M. Baier, G. Lutsch, D. A. Moss, K. Gast, D. Naumann, *J. Biol. Chem.* **2003**, *278*, 40481.
[18] S. Jain, J. B. Udgaonkar, *J. Mol. Biol.* **2008**, *382*, 1228.
[19] M. Morillas, D. L. Vanik, W. K. Surewicz, *Biochemistry* **2001**, *40*, 6982.
[20] J. T. Jarrett, P. T. Lansbury, Jr., *Cell* **1993**, *73*, 1055.
[21] K. Kuwajima, *Proteins* **1989**, *6*, 87.
[22] C. Redfield, *Methods* **2004**, *34*, 121.
[23] R. Gerber, A. Tahiri-Alaoui, P. J. Hore, W. James, *J. Biol. Chem.* **2007**, *282*, 6300.
[24] J. M. Andrews, C. J. Roberts, *J. Phys. Chem. B* **2007**, *111*, 7897.
[25] A. J. Modler, H. Fabian, F. Sokolowski, G. Lutsch, K. Gast, G. Damaschun, *Amyloid* **2004**, *11*, 215.
[26] I. V. Baskakov, G. Legname, S. B. Prusiner, F. E. Cohen, *J. Biol. Chem.* **2001**, *276*, 19687.
[27] J. W. Donovan, *Methods Enzymol.* **1973**, *27*, 497.
[28] P. Neudecker, P. Robustelli, A. Cavalli, P. Walsh, P. Lundstrom, A. Zarrine-Afsar, S. Sharpe, M. Vendruscolo, L. E. Kay, *Science* **2012**, *336*, 362.
[29] A. J. Baldwin, S. J. Anthony-Cahill, T. P. Knowles, G. Lippens, J. Christodoulou, P. D. Barker, C. M. Dobson, *Angew. Chem.* **2008**, *120*, 3433; *Angew. Chem. Int. Ed.* **2008**, *47*, 3385.
[30] N. Chakroun, S. Prigent, C. A. Dreiss, S. Noinville, C. Chapuis, F. Fraternali, H. Rezaei, *FASEB J.* **2010**, *24*, 3222.
[31] R. Gerber, K. Voitchovsky, C. Mitchel, A. Tahiri-Alaoui, J. F. Ryan, P. J. Hore, W. James, *J. Mol. Biol.* **2008**, *381*, 212.

